

# Influence of magnetic on ferroelectric ordering in LuMnO<sub>3</sub>

Bas B. Van Aken<sup>1,2,\*</sup> and Thomas T. M. Palstra<sup>2</sup>

<sup>1</sup>Department of Materials Science and Metallurgy, University of Cambridge, UK

<sup>2</sup>Solid State Chemistry Laboratory, Materials Science Centre, University of Groningen, The Netherlands

(Dated: July 26, 2018)

We have studied the influence of antiferromagnetic ordering on the local dielectric moments of the MnO<sub>5</sub> and LuO<sub>7</sub> polyhedra by measuring neutron powder diffraction patterns of LuMnO<sub>3</sub> at temperatures near  $T_N$ . We show that the coupling is weak, because the magnetic exchange coupling is predominantly in the *ab* plane of the MnO<sub>5</sub> trigonal bipyramids, and the electric dipole moments, originating in the LuO<sub>7</sub> polyhedra, are oriented along the hexagonal *c* axis. Anomalies in the dielectric properties near  $T_N$  are thus caused by the geometric constraints between the MnO<sub>5</sub> and the LuO<sub>7</sub> polyhedra.

PACS numbers:

Multiferroic magnetoelectrics are materials that combine ferroelectric and magnetic ordering. These materials are of fundamental and technological interest as coupling between different order parameters enables multiple ways to interact with these materials, such as pressure, electric and magnetic fields. In most ionic materials the Coulomb repulsion between ions results in centred (i.e. non-polar) crystal structures. Conventionally, only for ions with lone pairs and non-magnetic ions, sizeable dipole moments can exist<sup>1</sup>. For few extraordinary materials magnetic and electric dipolar order can coexist. The coupling between the magnetic and electric order must originate either from magnetic ordering affecting the electric dipoles via striction, or the displacements at the dipolar ordering changing the magnetic order. These interactions depend intimately on the coupling between the magnetic and electric building blocks of the 3D-crystal structure.

Recently the distorted perovskites BiMnO<sub>3</sub><sup>2,3</sup>, BiFeO<sub>3</sub><sup>4</sup> and also TbMnO<sub>3</sub><sup>5</sup> have been shown to combine magnetic and ferroelectric order. Another class of materials that combine magnetic and electric dipolar order are the hexagonal manganites with general formula AMnO<sub>3</sub>, which are antiferromagnetic and ferroelectric. Hexagonal AMnO<sub>3</sub> (h-AMnO<sub>3</sub>), in particularly YMnO<sub>3</sub>, has attracted interest for applications, for instance in non-volatile memory devices<sup>6</sup> or as ferroelectric gate electrode<sup>7</sup>. Progress has also been made in the understanding of the origin of the ferroelectric properties<sup>8</sup> and the coupling between the ferroelectric and antiferromagnetic order<sup>9,10</sup>. Fiebig *et al.* have shown that below the antiferromagnetic ordering temperature  $T_N$ , the ferroelectric domain walls, or twin boundaries, always act as antiferromagnetic (AFM) domain walls as well. Furthermore, AFM domain walls also exist in the bulk of the ferroelectric (FE) domains. This suggests that not the orientation of the FE order and the AFM order are linked, but that the transition from one FE orientation to the other forces or accommodates a transition in the AFM order<sup>9,11</sup>. The coupling between electric and magnetic ordering requires detailed knowledge of the crystal structure. Unfortunately, there are conflicting results in the literature on the atomic positions when

comparing neutron powder diffraction (NPD) and single crystal X-ray diffraction (SXD). Neutron diffraction results show anomalous variations in the bond lengths<sup>12,13</sup> with temperature.

The crystal structure of h-AMnO<sub>3</sub> has two major differences compared with the perovskite structure. Firstly, the Mn<sup>3+</sup> ions (high spin 3d<sup>4</sup>) are located at the centre of a trigonal bipyramidal instead of an octahedron. The resulting crystal field splits the 3d levels in three energy levels, in order of increasing energy: *xz* and *yz*; *xy* and  $x^2-y^2$ ; and  $3z^2-r^2$ . Consequently, Mn<sup>3+</sup> 3d<sup>4</sup> has no partially filled degenerate levels and is therefore *not* Jahn-Teller active<sup>14</sup>. Density of states calculations show some mixing between the Mn 3d and O 2p levels.<sup>8</sup> Secondly, the MnO<sub>5</sub> polyhedra are corner linked in sheets, separated by a layer of A ions. This contrasts the MnO<sub>6</sub> 3D network in perovskite manganites. As a result, h-AMnO<sub>3</sub> is pseudo-layered, reflected for instance in the Mn spin being in the *xy* plane even above  $T_N$ <sup>14,15,16</sup>.

To explain the how the AFM and FE order are linked, we studied the temperature dependence of the crystal structure of LuMnO<sub>3</sub> around the antiferromagnetic ordering temperature,  $T_N = 88$  K, which is much lower than the FE ordering temperature,  $T > 573$  K<sup>17</sup>. Furthermore, we discuss the relation between the ionic radius of the A ion  $r_A$  and the crystal structure.

## I. TEMPERATURE DEPENDENCE OF LuMnO<sub>3</sub>

LuMnO<sub>3</sub> has been prepared with standard solid state synthesis. Neutron powder diffraction has been performed at the Polaris time-of-flight instrument at ISIS. The data have been refined using the GSAS package<sup>18</sup>, including isotropic temperature factors. Sample quality has been checked by measuring a neutron powder diffraction pattern at ambient temperature. No reflections from impurity phases could be detected and the refined structure was in good agreement with single crystal data<sup>19</sup>. Temperature dependent measurements, between 40 and 120 K, were performed at the same beam line, using a standard Orange cryostat. Typically quality factors

for the refinements are  $\chi^2 = 2.963$ ,  $R(F^2) = 4.79\%$  and  $R_p = 1.74\%$  for 47 variables.

Fig. 1(a) shows the crystal structure of hexagonal manganite. It consists of non-connected layers of  $\text{MnO}_5$  trigonal bipyramids, that are corner-linked by in-plane oxygen ions,  $\text{O}3$  and  $\text{O}4$ . The apical oxygen ions,  $\text{O}1$  and  $\text{O}2$ , form two close packed layers separated by a distorted layer of  $\text{A}^{3+}$  ions. In Fig. 1(b) a cross-section through the  $z \sim 0$  plane is given. The oxygen positions  $\text{O}1$  and  $\text{O}2$  are similar to the  $\text{Mn}$  positions, albeit with  $z \sim \pm \frac{1}{6}$ . The  $\text{A}$  site ions  $\text{A}1$  ( $\text{A}2$ ) are located exactly above the positions  $\text{O}3$  ( $\text{O}4$ ). In the next  $\text{Mn}$  ions containing layer ( $z \sim \frac{1}{2}$ ), the  $\text{Mn}$ ,  $\text{O}1$  and  $\text{O}2$  positions are located at  $x$  (Fig. 1(b)).

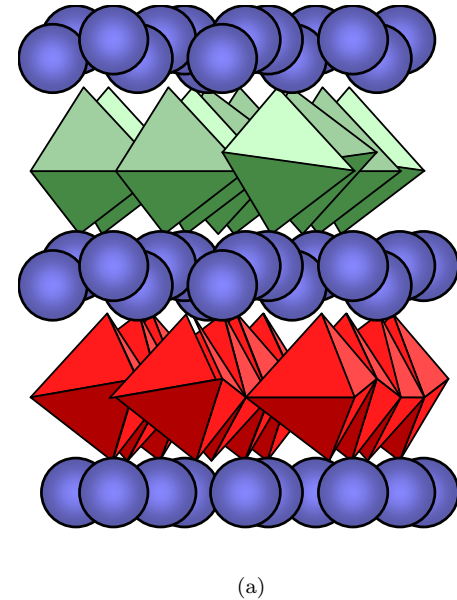
The spacegroup of hexagonal  $\text{LuMnO}_3$  in the ferroelectric phase is  $P6_3cm$ . The hexagonal unit cell contains six formula units; there are seven inequivalent positions with 10 refinable parameters. Since all symmetry elements are parallel to the  $c$  axis, all  $z$  coordinates are “free”. For practical reasons, we have chosen to fix  $z_{\text{Mn}} = 0$ . The atomic positions are listed in Table I.

TABLE I: The atomic positions of hexagonal manganite  $\text{AMnO}_3$ .  $m$  is the multiplicity of the site.

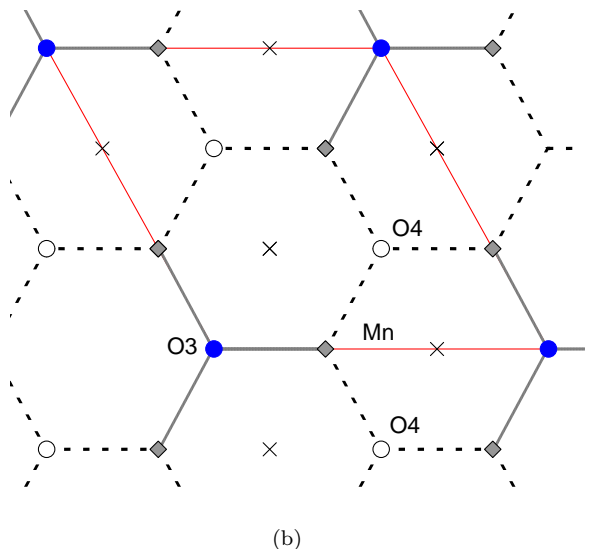
| atom        | $x$ (-)                          | $y$ (-)       | $z$ (-)                           | $m$ |
|-------------|----------------------------------|---------------|-----------------------------------|-----|
| $\text{A}1$ | 0                                | 0             | $z_{\text{A}1} \sim \frac{1}{4}$  | 2   |
| $\text{A}2$ | $\frac{1}{3}$                    | $\frac{2}{3}$ | $z_{\text{A}2} \sim \frac{1}{4}$  | 4   |
| $\text{Mn}$ | $x_{\text{Mn}} \sim \frac{1}{3}$ | 0             | $z_{\text{Mn}} = 0$               | 6   |
| $\text{O}1$ | $x_{\text{O}1} \sim \frac{1}{3}$ | 0             | $z_{\text{O}1} \sim \frac{1}{6}$  | 6   |
| $\text{O}2$ | $x_{\text{O}2} \sim \frac{1}{3}$ | 0             | $z_{\text{O}2} \sim -\frac{1}{6}$ | 6   |
| $\text{O}3$ | 0                                | 0             | $z_{\text{O}3} \sim 0$            | 2   |
| $\text{O}4$ | $\frac{1}{3}$                    | $\frac{2}{3}$ | $z_{\text{O}4} \sim 0$            | 4   |

In Fig. 2 the lattice parameters has been plotted versus the temperature. The  $a$  axis decreases with decreasing temperature at a rate of  $8 \cdot 10^{-6} \text{ K}^{-1}$ . The lattice parameter  $c$  is nearly independent of  $T$ , although a small discontinuity in  $c$  ( $\sim 0.001 \text{ \AA}$ ) can be seen near  $T_N$ . SXD data at  $295 \text{ K}^{19}$ ,  $a = 6.038(1) \text{ \AA}$ , are in agreement with the extrapolation of Fig. 2. Thermal expansion data have been reported on powdered  $\text{YMnO}_3$  samples at higher temperatures<sup>20</sup>. The expansion coefficient  $\sim 7 \cdot 10^{-7} \text{ K}^{-1}$  obtained from these data is one order of magnitude smaller than the value we find.

Compared to the paraelectric centrosymmetric structure, the  $\text{MnO}_5$  bipyramids are rotated along an axis through the  $\text{Mn}$  ion and parallel to the  $\text{O}4$ - $\text{O}4$  bond. This buckling moves the  $\text{O}3$  ( $\text{O}4$ ) ions up (down) along the  $z$ -axis and moves the  $\text{O}1$  ( $\text{O}2$ ) ions at ( $\sim \frac{1}{3}, 0, \pm \frac{1}{6}$ ) along the  $x$ -axis. Fig. 3 shows the  $T$  dependence of the apical oxygen positions  $\text{O}1$  and  $\text{O}2$  of  $\text{LuMnO}_3$ , plotted as the absolute difference with their paraelectric position at  $x = \frac{1}{3}$ . The  $x$  coordinate of these oxygen ions is a measure for the buckling of the  $\text{MnO}_5$  trigonal bipyramidal, but small changes in  $x_{\text{O}1}$  and  $x_{\text{O}2}$  do not have a significant effect on the  $\text{Mn}-\text{O}1$  and  $\text{Mn}-\text{O}2$  bond lengths. The



(a)



(b)

FIG. 1: (a) View perpendicular to the  $c$  axis of the crystal structure of  $\text{AMnO}_3$ . The trigonal bipyramids represent the  $\text{MnO}_5$  and the circles the  $\text{A}$  ions. This sketch highlights the stacking of the  $\text{MnO}_5$  layers. (b) Sketch of the  $z=0$  layer of  $\text{LuMnO}_3$ , showing the two inequivalent  $\text{Mn} - \text{O}$  bonds.  $\text{Mn}$ ,  $\text{O}3$  and  $\text{O}4$  are shown as grey diamonds, closed and open circles, respectively.  $\text{Mn} - \text{O}3$  and  $\text{Mn} - \text{O}4$  bonds are indicated by solid and dashed lines, respectively. The thin line outlines the unit cell.

linear fits suggest that the buckling might reduce with decreasing  $T$ , but the slope and its error are the same order of magnitude. The angle of the line through  $\text{O}1$  and  $\text{O}2$  with the  $xy$ -plane changes from  $84.7^\circ$  at  $T = 120 \text{ K}$  to  $84.8^\circ$  at  $T = 40 \text{ K}$ . We conclude that there is hardly any change in the buckling of the  $\text{MnO}_5$  layers with tem-

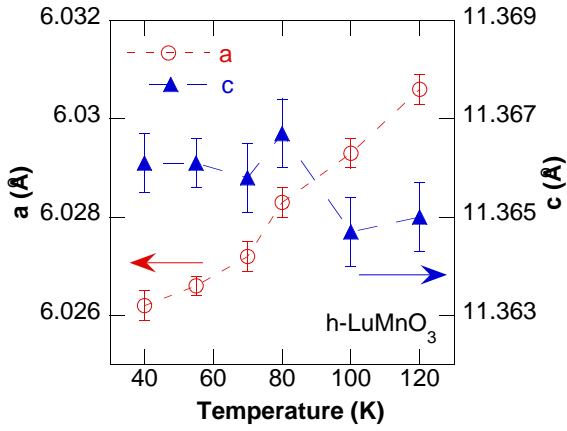


FIG. 2: Temperature dependence of lattice parameters of LuMnO<sub>3</sub>.

perature.

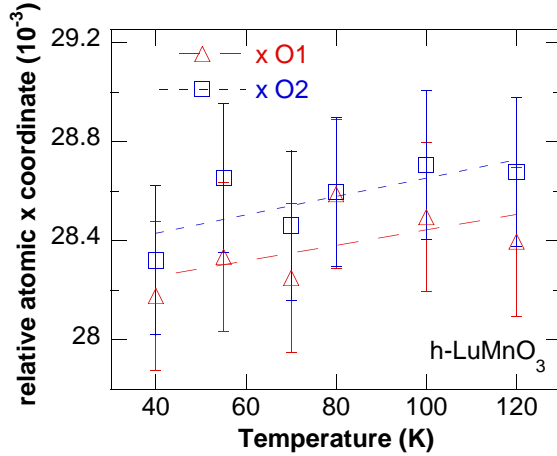


FIG. 3: Temperature dependence of the  $x$  coordinate of the apical oxygen positions of LuMnO<sub>3</sub>. The absolute difference with the paraelectric position at  $x = \frac{1}{3}$  is plotted. Triangles and squares depict O1 and O2, respectively. The dashed lines are least squares linear fits.

The out-of-plane A1–O3 and A2–O4 bond lengths are calculated using:

$$A1-O3 = c(z_{A1} - z_{O3}) \quad (1)$$

and

$$A2-O4 = c(z_{A2} - z_{O4}). \quad (2)$$

Since the temperature dependence of lattice parameter  $c$  is negligible, the  $T$  dependence of these bond lengths depend only on the  $T$  dependence of the  $z$  coordinates. We found in our refinements that the  $T$  dependencies of these  $z$  coordinates have strong positive correlations. Any changes in any of the  $z$  coordinates is mimicked closely by its companion. Therefore, the Lu1–O3 and Lu2–O4 bond lengths show no dependence on temperature.

Each Mn ion has two Mn–O4 bonds and one Mn–O3 bond as is shown in Fig. 1(b). The in-plane Mn–O3 bond length is given by

$$Mn-O3 = \sqrt{a^2 x_{Mn}^2 + c^2 z_{O3}^2} \sim a x_{Mn}, \quad (3)$$

where in the approximation the effect of  $z_{O3} \neq 0$  can be ignored, since the partial derivatives are proportional to the magnitude of  $x_{Mn}$  and  $z_{O3}$ . The other in-plane bond length is given by

$$Mn-O4 = \sqrt{a^2 \{(x_{Mn} - 1/2)^2 + (\sqrt{3}/6)^2\} + c^2 z_{O4}^2}. \quad (4)$$

Mn–O3 and Mn–O4 depend both on lattice parameter  $a$  and on the  $x$  coordinate of the Mn ion. We can write  $x_{Mn} = \frac{1}{3} - \delta$ , where  $\delta$  is the displacement of the Mn ion along the  $x$  axis from its paraelectric position at  $(\frac{1}{3}, 0, 0)$ , see Fig. 4.

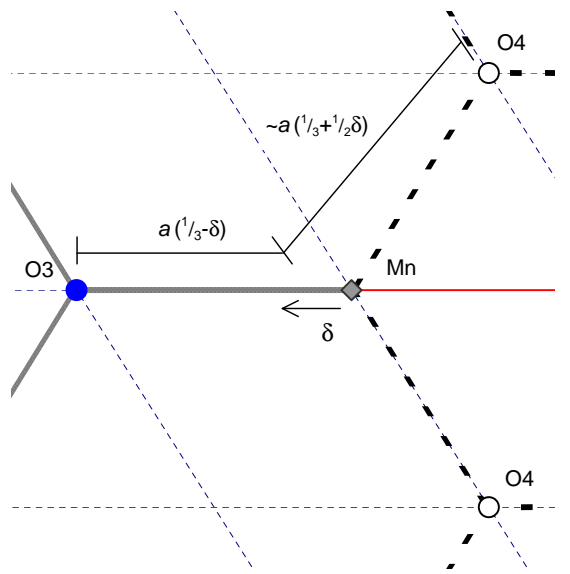


FIG. 4: Sketch of the relation of the length of the two inequivalent in-plane Mn–O bonds, showing the effect of an in-plane Mn displacement. Symbols are the same as in Fig. 1(b). Thin dashed lines are lines parallel to the unit cell axes at  $\frac{1}{3}a$  intervals to guide the eye.

Then, applying  $x_{Mn} = \frac{1}{3} - \delta$ , Mn–O3 equals  $a(\frac{1}{3} - \delta)$  and Mn–O4 equals

$$\begin{aligned} Mn-O4 &= \sqrt{a^2 \{(1/6 + \delta)^2 + 1/12\} + c^2 z_{O4}^2} \sim \\ &\sim a(1/3 + 1/2\delta), \end{aligned} \quad (5)$$

where the effect of  $z_{O4} \neq 0$  and  $\delta^2$  is negligible.

From these approximate formulae we can see that a change, of  $-\delta a$ , in the length of the Mn–O3 bond length,

due to a displacement  $\delta$  of the Mn ion, is always accompanied with a change in the length of the Mn–O4 bond of opposite sign and half the magnitude ( $\pm \frac{1}{2}\delta a$ ). These in-plane Mn–O bond lengths are plotted against temperature in Fig. 5. Local extrema near  $T_N$  are observed with the maximum value for Mn–O3 smaller than the minimum for Mn–O4. Below and above  $T_N$  the difference increases between the in-plane bond lengths. However the observed differences are not large, at most 0.041 Å.

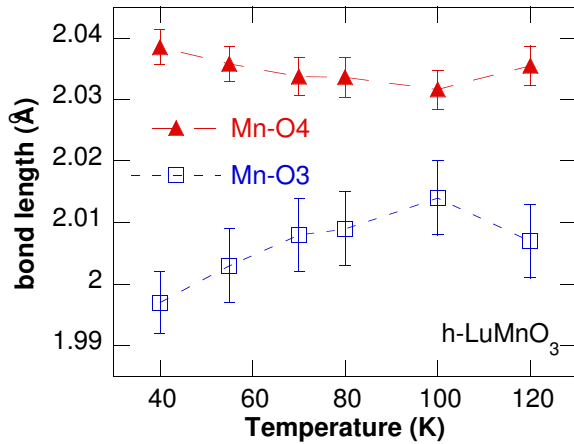


FIG. 5: Temperature dependence of in-plane Mn–O bond lengths around  $T_N = 88$  K.

The out-of-plane Mn–O bond lengths are given by

$$\text{Mn–O}_i = \sqrt{a^2(x_{Mn} - x_{O_i})^2 + c^2z_{O_i}^2} \sim c z_{O_i}; (i = 1, 2) \quad (6)$$

where the  $x$  components are neglected in the approximation, since  $x_{Mn} - x_{O_i} \ll z_{O_i}; (i = 1, 2)$ . The out-of-plane bond lengths also show local extrema near  $T_N$ , but the changes are less pronounced than for the in-plane bond lengths. The difference between the inequivalent out-of-plane Mn–O bond lengths is smaller than 0.02 Å for all  $T$ .

The out-of-plane bond lengths are much shorter than the in-plane bond lengths, respectively  $\sim 1.87$  Å and  $\sim 2.02$  Å. This is related to the crystal field splitting of the Mn 3d orbitals, with the unoccupied  $3z^2 - r^2$  orbital in the out-of-plane direction. The antibonding character of the Mn 3d - O 2p interaction elongates the in-plane bond lengths<sup>14</sup>.

We note that with SXD<sup>19,21,22,23</sup>, it is found that the Mn–O4 bond length is smaller than the Mn–O3 bond length, whereas here we find that Mn–O4 is larger than Mn–O3. However, the difference between the inequivalent in-plane bond lengths is small ( $< 0.05$  Å). The out-of-plane Mn–O bond lengths are in line with the SXD data, and the difference between the inequivalent out-of-plane bond lengths is small ( $< 0.02$  Å) in agreement with the SXD data. Other NPD experiments on the crystal structure of hexagonal manganites in the literature report larger differences between the in-plane or

the out-of-plane Mn–O bond lengths. For instance, Katsumi *et al.* report on LuMnO<sub>3</sub> at 300 K and find out-of-plane bond lengths of 1.98 Å and 1.78 Å<sup>13</sup>. Muñoz *et al.* find for YMnO<sub>3</sub> at room temperature a difference between in-plane bond lengths  $\Delta_{\text{in-plane}}$  of 0.1 Å<sup>12</sup>. Also older structure reports using SXD show large differences between in-plane Mn–O bond lengths or out-of-plane Mn–O bond lengths. Yakel reports  $\Delta_{\text{in-plane}} = 0.08$  Å and  $\Delta_{\text{out-of-plane}} = 0.09$  Å for LuMnO<sub>3</sub><sup>24</sup>. Isobe reports  $\Delta_{\text{in-plane}} = 0.048$  Å and  $\Delta_{\text{out-of-plane}} = 0.058$  Å for YbMnO<sub>3</sub> at  $T = 295$  K<sup>25</sup>. These SXD experiments however did not include reflections from all regions of  $hkl$  space, which is necessary for SXD on non-centrosymmetric crystals.

In the previous section, we have discussed the temperature dependence of the bond lengths. Now, we will investigate whether the observed changes have any effect on the local dipole moments and the macroscopic ferroelectric moment. In the remainder of this article, we will define the local dipole moment associated with a cation site as the distance between the centre of gravity of the nearest neighbour O ions and the cation site.

In Fig. 5 we have shown that the in-plane Mn–O bond lengths show local extrema near  $T_N$ , with the difference between them smallest at  $T_N$ . This means that also their contribution to the local dipole moments on the Mn site is smallest at  $T_N$ . The space group symmetry relates the local dipole moment created by the small in-plane displacement of the Mn ion to the local dipole moments originating from the other two Mn ions on the same plane in the unit cell. Due to the sixfold screw axis, the local dipole moments are rotated over an angle of 120° with respect to each other. As a result, there cannot be any contribution to the macroscopic ferroelectric moment by the in-plane displacements.

The difference between the out-of-plane Mn–O1 and Mn–O2 bond lengths create a small local dipole moment  $< 0.02$  Å from the Mn coordination. These local dipole moments are parallel to the  $c$  axis and they are not cancelled by the crystal symmetry. However larger local dipole moments originate from the Lu1 and Lu2 coordination<sup>8</sup>. The local dipole moments from the Lu coordination are at least an order of magnitude larger than the ones from the Mn coordination.

The local dipole moments associated with the LuO<sub>8</sub> polyhedra are shown in Fig. 6. The calculation of the centre of gravity of the oxygen polyhedra includes the seven ions at  $\sim 2.4$  Å and the one ion at  $\sim 3.2$  Å. Note that the local dipole moments from the Lu2 coordination are antiparallel with the ones from the Lu1 coordination.

From Fig. 6 it is clear that cooling through the Néel transition has no significant influence on the local dipole moments of LuMnO<sub>3</sub>. However, we have shown in Fig. 5 that the local environment around the Mn ions does change. Since the Mn spins are in-plane<sup>14</sup>, even above  $T_N$ , the magnetic ordering transition at  $T_N$  is expected to have the largest effect on the in-plane Mn–O bond lengths. The ferroelectricity on the other hand depends

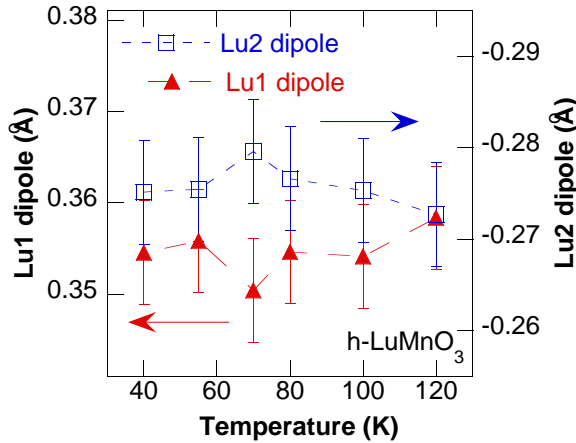


FIG. 6: Temperature dependence of LuMnO<sub>3</sub> of the local dipole moments from the Lu1 and the Lu2 polyhedra near  $T_N = 88$  K. Note that the right axis is reversed.

mostly on the out-of-plane Lu–O bond lengths<sup>8</sup>. Although the oxygen ions involved are the same, O<sub>3</sub> and O<sub>4</sub>, the Mn–O bond lengths change mostly by a displacement  $\delta$  of the Mn ion along the  $x$  axis, whereas the out-of-plane Lu–O bond lengths change because of an opposite movement of the Lu1 (Lu2) and O<sub>3</sub>(O<sub>4</sub>) ions along the  $c$  axis. We conclude that there is no significant coupling between the ferroelectric moment of LuMnO<sub>3</sub> and the antiferromagnetic ordering temperature. This is in agreement with the conclusions from Ref. 9.

## II. RARE EARTH IONIC RADIUS

In the second part of this article we will discuss the influence of the rare earth ions, by their ionic radius  $r_A$ , on the local dipole moments. The data used in this analysis has been taken from Refs. [21] (YMnO<sub>3</sub>); [22] (ErMnO<sub>3</sub>); [23] (YbMnO<sub>3</sub>) and [19] (LuMnO<sub>3</sub>).

In Fig. 7, the lattice parameters  $a$  and  $c$  at  $T = 295$  K are plotted against  $r_A$ . The values of  $r_A$  have been taken from Shannon and Prewitt<sup>26</sup>. We observe that with increasing  $r_A$  the lattice parameters increase. From LuMnO<sub>3</sub> to YMnO<sub>3</sub> lattice parameter  $a$  increases linearly, with a total increase of  $\sim 1.7\%$ . Lattice parameter  $c$  has a smaller increase of about  $0.5\%$ . We can clearly see from these data that the influence of  $r_A$  is larger on the in-plane lattice parameter than on the out-of-plane lattice parameter.

The crystal structure can be regarded as a stacking of hexagonally packed oxygen layers and A ion layers. One expects that O–O bond lengths are  $\sim 2.8$  Å, ( $r_O = 1.4$  Å) and A–O bond lengths are  $\sim 2.4$  Å, ( $r_A \sim 1.05$  Å). For instance, in LaMnO<sub>3</sub> the average O–O and La–O bond length (in the fcc-like closed packed OO and AO layers) is  $\sim 2.7$  Å ( $r_{La} = 1.2$  Å). The observed values for the inter-plane A–O<sub>1</sub> and A–O<sub>2</sub> bond lengths in hexagonal AMnO<sub>3</sub> (not shown here) are consistent with

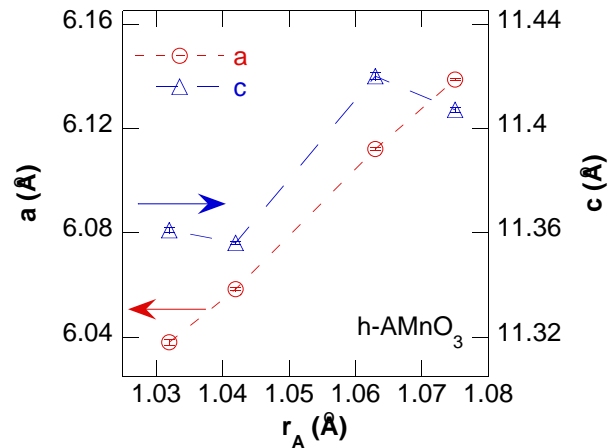


FIG. 7: Lattice parameters for hexagonal AMnO<sub>3</sub> as a function of  $r_A$  (A=Lu, Er, Yb and Y) at  $T = 295$  K.

the expected values. Likewise the observed increase with increasing  $r_A$  of the A–O<sub>1</sub> and A–O<sub>2</sub> bond lengths (on average  $1.6\%$ ) is in excellent agreement with the increase of  $a$  with  $r_A$ .

We note that in hexagonal AMnO<sub>3</sub> both the hexagonally packed O layers at  $z \approx \pm \frac{1}{6}$  and the MnO layers at  $z \approx 0$  have intra-plane O–O distances of  $\sim 3.6$  Å. Similarly, the in-plane A–A distances are also  $\sim 3.6$  Å. This is in contrast with the intra-plane bond lengths in pseudo-cubic perovskites. These anomalously large "bond lengths" can be understood, by considering the way the layers are stacked. Starting at the MnO layer at  $z = 0$ , the stacking order is MnO–O–A–O–MnO with layer spacings of about  $\frac{2}{12}c$ ,  $\frac{1}{12}c$ ,  $\frac{1}{12}c$  and  $\frac{2}{12}c$ . One can visualise that the A ion layer (at  $z \approx \frac{1}{4}$ ) is clamped between the closed packed O layer (at  $z \approx \frac{1}{6}$  and  $z \approx \frac{1}{3}$ ). This will enlarge the spacing of the O and A ions in those layers. The larger the radius of the A ions, the more the O ions are pushed apart. However, the O–O bond length between the two neighbouring O layers at  $z \approx \frac{1}{6}$  and  $z \approx \frac{1}{3}$  is reduced to  $\sim 2.8$  Å, which corresponds to the value one expects ( $2 \times r_O$ ). In this simple model, changes in  $r_A$  can be accommodated completely by a change in the in-plane bond lengths and lattice parameter  $a$ .

The decreasing distances in the  $ab$  plane with decreasing  $r_A$  should also be reflected in the in-plane Mn–O bond lengths. The change of  $\sim 1.6\%$  is in good agreement with the observed change of  $a$  with decreasing  $r_A$ . Possible changes in the out-of-plane Mn–O bonds are too small to be resolved within the scatter and error bars of the experiments. However, we observe a distinct relation between the A<sub>1</sub>–O<sub>3</sub> and A<sub>2</sub>–O<sub>4</sub> bond lengths and  $r_A$ , as shown in Fig. 8.

The short A<sub>1</sub>–O<sub>3</sub> and A<sub>2</sub>–O<sub>4</sub> bonds increase by  $3.6\%$  and  $2.3\%$  with increasing  $r_A$ . Therefore, the "extra long" out-of-plane A–O bond lengths should decrease with increasing  $r_A$ , since  $c$  is almost constant. Consequently, the dipoles of the A polyhedra decrease with increasing  $r_A$ .

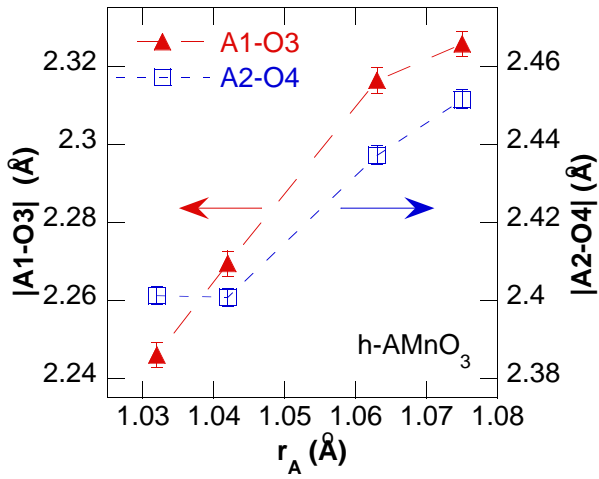


FIG. 8: out-of-plane A–O bond lengths as a function of  $r_A$ .

The increase in dipole moment from Y ( $r_A = 1.075$  Å) to Lu ( $r_A = 1.032$  Å) is about 10% as shown in Fig. 9.

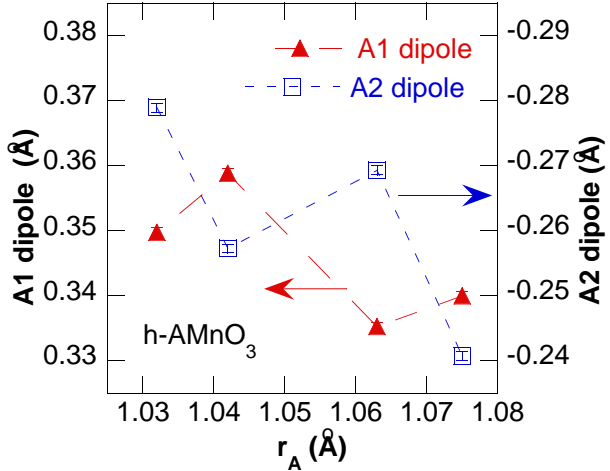


FIG. 9: Dipole moments of the A1 and A2 polyhedra of h-AMnO<sub>3</sub>. Note that the A2 dipole is plotted on a reverse scale. Both dipoles tend to increase with decreasing  $r_A$ .

The transition from the paraelectric centrosymmetric to the ferroelectric non-centrosymmetric structure consists of two atomic displacements. The first is the buckling of the MnO<sub>5</sub> network, displacing O1 and O2 in the  $xy$  plane and O3 and O4 along the  $z$  axis. The second is the alternate displacement of the A1 and A2 ions along the  $z$  axis away from the  $z = \frac{1}{4}$  mirror plane<sup>8</sup>. Formally, it has been shown that these atomic displacements consist of two modes. Firstly, there is a K<sub>3</sub> mode, which changes the symmetry but can inherently not create a macroscopic ferroelectric moment. Secondly, there is a  $\Gamma$  mode, which does not change the space group symmetry, but introduces the macroscopic ferroelectricity<sup>27,28</sup>. To see which of these two modes is influenced more by chemical substitution, we have plotted in Fig. 10 the  $z$

coordinates of the A1 and the O3 sites. Both  $z$  coordinates of A1 and O3 are about 0.02 $c$  away from their centrosymmetric equilibrium position. Clearly, the changes in the  $z$  coordinate of O3 site are much larger than the changes in the  $z$  coordinate of the A1 site. The data in Fig. 10 therefore show that upon chemical substitution of the A site the buckling increases with decreasing  $r_A$ , which results in an increase of the deviation from the centrosymmetric positions. The displacement of the A ions from the mirror plane is more or less constant. This is supported by the changes in the  $x$  coordinates of the O1 and O2 sites. Both are about 0.025 $a$  off their symmetric position at  $x = \frac{1}{3}$  and this deviation becomes larger by  $\sim 10\%$  from R=Y to R=Lu. We conclude that the change in the local dipole moment is caused by atomic rearrangement and not by expansion of the unit cell.

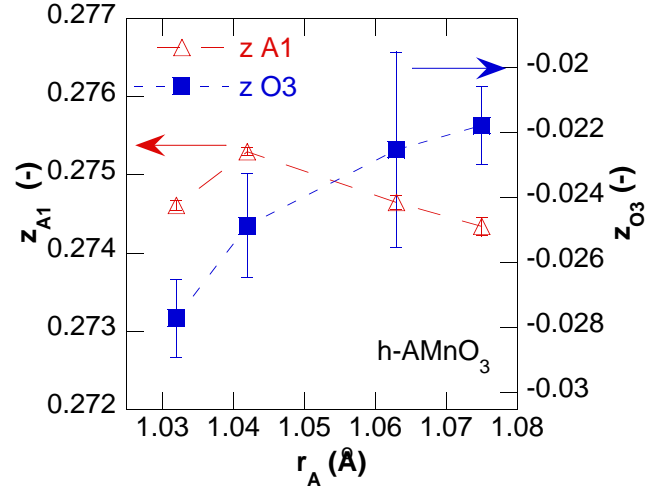


FIG. 10: Fractional  $z$  coordinates of the A1 and O3 position (0, 0,  $z$ ) versus  $r_A$ . Clearly the  $z$  coordinates deviate more from their equilibrium positions, respectively  $z = \frac{1}{4}$  and  $z = 0$ , with decreasing  $r_A$ .

The ferroelectric transition temperatures for these materials have been reported, but different authors report completely different values or only "higher than" values. Furthermore, there are indications that the ferroelectric ordering temperature and the non-centrosymmetric to centrosymmetric phase transition temperature are different by several hundreds degrees<sup>27,29</sup>. It is therefore not possible to relate the magnitude of the local dipole moments or the total dipole moment to the ferroelectric ordering temperature.

The effect of changing  $r_A$  can be summarised as follows. A decrease in  $r_A$  will reduce the "normal" A–O bond lengths. This will change the in-plane Mn–O bond lengths too. These changes are accompanied by an increased buckling of the MnO<sub>5</sub> bipyramids, parameterised by  $x_{O1}$ ,  $x_{O2}$ ,  $z_{O3}$  and  $z_{O4}$ . The changes in the oxygen  $z$  coordinates induce an increase in the difference between the short and long A1–O3 and A2–O4 bond lengths. This increases the dipole moments from the A1 and A2 coordinations with decreasing  $r_A$ . However, the antipar-

allel coupling between the local dipole moments at the A1 and the A2 site prevents a clear effect on the total dipole moment.

In conclusion, the hexagonal  $AMnO_3$  compounds exhibit both antiferromagnetic and ferroelectric order. The magnetic exchange and spins are confined in the basal plane, whereas the dielectric moments originate predominantly from displacements parallel to the  $c$ -axis. Con-

sequently, the distortions due to magnetostrictive effects and dipolar ordering are only weakly coupled.

We thank Ron Smith, Anne Dros and Auke Meetsma for experimental assistance. This work is supported by the ‘Stichting voor Fundamenteel Onderzoek der Materie (FOM)’, NWO for neutron beam time at ISIS and the EU Marie Curie Fellowship.

\* Electronic address: bbv20@cam.ac.uk

- <sup>1</sup> N. A. Hill, *J. Phys. Chem. B* **104**, 6694 (2000).
- <sup>2</sup> A. Moreira dos Santos, A. K. Cheetham, T. Atou, Y. Syono, Y. Yamaguchi, K. Ohoyama, H. Chiba, and C. N. R. Rao, *Phys. Rev. B* **66**, 064425 (2002).
- <sup>3</sup> R. Seshadri and N. A. Hill, *Chem. Mater.* **13**, 2892 (2003).
- <sup>4</sup> J. Wang, J. B. Neaton, H. Zheng, V. Nagarajan, S. B. Ogale, B. Liu, D. Viehland, V. Vaithyanathan, D. Schlom, U. V. Waghmare, N. A. Spaldin, K. M. Rabe, M. Wuttig, and R. Ramesh, *Science* **299**, 1719 (2003).
- <sup>5</sup> T. Kimura, T. Goto, H. Shintani, K. Ishizaka, T. Arima, and Y. Tokura, *Nature* **426**, 55 (2003).
- <sup>6</sup> N. Fujimura, T. Ishida, T. Yoshimura, and T. Ito, *Appl. Phys. Lett.* **69**, 1011 (1996).
- <sup>7</sup> D. Ito, N. Fujimura, T. Yoshimura, and T. Ito, *J. Appl. Phys.* **93**, 5563 (2003).
- <sup>8</sup> B. B. Van Aken, T. T. M. Palstra, A. Filippetti, and N. A. Spaldin, *Nature Materials* **3** (2004), accepted.
- <sup>9</sup> M. Fiebig, T. Lottermoser, D. Fröhlich, A. V. Goltsev, and R. V. Pisarev, *Nature* **419**, 818 (2002).
- <sup>10</sup> E. Hanamura, K. Hagita, and Y. Tanabe, *J. Phys.: Cond. Matt.* **15**, L103 (2003).
- <sup>11</sup> A. V. Goltsev, R. V. Pisarev, T. Lottermoser, and M. Fiebig, *Phys. Rev. Lett.* **90**, 177204 (2003).
- <sup>12</sup> A. Muñoz, J. A. Alonso, M. J. Martínez-Lope, M. T. Casáis, J. L. Martínez, and M. T. Fernández-Díaz, *Phys. Rev. B* **62**, 9498 (2000).
- <sup>13</sup> T. Katsufuji, M. Masaki, A. Machida, Y. Moritomo, K. Kato, E. Nishibori, M. Takata, M. Sakata, K. Ohoyama, K. Kitazawa, and H. Takagi, *Phys. Rev. B* **66**, 134434 (2002).
- <sup>14</sup> B. B. Van Aken, J.-W. G. Bos, R. A. De Groot, and T. T. M. Palstra, *Phys. Rev. B* **63**, 125127 (2001).

- <sup>15</sup> T. Lottermoser, M. Fiebig, D. Fröhlich, S. Leute, and K. Kohn, *J. Magn. Magn. Mater.* **226-230**, 1131 (2001).
- <sup>16</sup> T. Lottermoser, Ph.D. thesis, Universität Dortmund (2002).
- <sup>17</sup> E. F. Bertaut, E. F. Forrat, and P. Fang, *C. R. Acad. Sci.* **256**, 1958 (1963).
- <sup>18</sup> A. C. Larson and R. B. Von Dreele, *General structure analysis system (GSAS)*, Los Alamos National Laboratory Report LAUR 86-748 (1994).
- <sup>19</sup> B. B. Van Aken, A. Meetsma, and T. T. M. Palstra, *Acta Crystallogr. Sect. E* **57**, i101 (2001), cond-mat/0106298.
- <sup>20</sup> G. Lescano, F. M. Figueiredo, F. M. B. Marques, and J. Schmidt, *J. Eur. Ceram. Soc.* **21**, 2037 (2001).
- <sup>21</sup> B. B. Van Aken, A. Meetsma, and T. T. M. Palstra, *Acta Crystallogr. Sect. C* **57**, 230 (2001).
- <sup>22</sup> B. B. Van Aken, A. Meetsma, and T. T. M. Palstra, *Acta Crystallogr. Sect. E* **57**, i38 (2001), cond-mat/0106298.
- <sup>23</sup> B. B. Van Aken, A. Meetsma, and T. T. M. Palstra, *Acta Crystallogr. Sect. E* **57**, i87 (2001), cond-mat/0106298.
- <sup>24</sup> H. L. Yakel, W. C. Koehler, E. F. Bertaut, and E. F. Forrat, *Acta Crystallogr.* **16**, 957 (1963).
- <sup>25</sup> M. Isobe, N. Kimizuka, M. Nakamura, and T. Mohri, *Acta Crystallogr. Sect. C* **47**, 423 (1991).
- <sup>26</sup> R. D. Shannon and C. T. Prewitt, *Acta Crystallogr.* **A32**, 751 (1976).
- <sup>27</sup> T. Lonkai, D. G. Tomuta, R. W. A. Hendrikx, U. Amann, J. Ihringer, D. M. Többens, and J. A. Mydosh, *Development of the high temperature phase of hexagonal manganites*, submitted to *Phys. Rev. B*.
- <sup>28</sup> T. Lonkai, Ph.D. thesis, University of Tübingen (2003).
- <sup>29</sup> K. Łukaszewicz and J. Karut-Kalicinska, *Ferroelectrics* **7**, 81 (1974).